Efficacy and mechanism of actions of cipargamin as an antibabesial drug candidate

Authors

Hang Li[1#], Shengwei Ji[1,2#], Nanang R. Ariefta[1], Eloiza May S. Galon[3], Shimaa AES El-Sayed[1,4], Lijun Jia[2], Yoshifumi Nishikawa[1], Mingming Liu[1,5]*, Xuenan Xuan[1]*

Affiliations

[1]National Research Center for Protozoan Diseases, Obihiro University of Agriculture Veterinary Medicine, Inada-cho, Obihiro, Japan

[2]Department of Veterinary Medicine, Agriculture College of Yanbian University, Yanji, China

[3]College of Veterinary Medicine and Biomedical Sciences, Cavite State University, Indang, Philippines

[4]Department of Biochemistry and Molecular Biology, Faculty of Veterinary Medicine, Mansoura University, Egypt

[5]School of Basic Medicine, Hubei University of Arts and Science, Xiangyang, China

*** Correspondence:** Mingming Liu; Xuenan Xuan

Address: Longzhong Road No.296, Xiangyang, China; Nishi 11 Minami 39 Chome, Obihiro, Hokkaido

Telephone number: +8618904416800; +8109079036369

E-mail address: lmm_2010@hotmail.com; gen@obihiro.ac.jp

Competing interest: The authors have declared that no conflict of interest exists.

# These authors contributed equally to this work.

Abstract

Babesiosis is a disease brought on by intraerythrocytic parasites of the genus *Babesia*. Current chemotherapies are accompanied by side effects and parasite relapse. Therefore, it is crucial to develop highly effective drugs against *Babesia*. Cipargamin (CIP) has shown inhibition against apicomplexan parasites, mainly *Plasmodium* and *Toxoplasma*. This study evaluated the growth-inhibiting properties of CIP against *Babesia* spp. and investigated the mechanism of CIP on *B. gibsoni*. The half inhibitory concentration (IC_{50}) values of CIP against the *in vitro* growth of *B. bovis* and *B. gibsoni* were 20.2 ± 1.4 nM and 69.4 ± 2.2 nM, respectively. CIP significantly inhibited the growth of *B. microti* and *B. rodhaini in vivo.* Resistance was conferred by L921V and L921I mutations in *Bg*ATP4, which reduced the sensitivity to CIP by 6.1- and 12.8-fold. An *in silico* investigation revealed reductions in affinity for CIP binding to *Bg*ATP4^{L921V} and *Bg*ATP4^{L921I} compared to *Bg*ATP4^{WT}. In this study, we characterized the efficacy of CIP against *Babesia* spp. by investigating the mechanistic basis for the resistance to CIP conferred by mutations in the *Bg*ATP4. Our findings present a promising starting point for the establishment of new therapeutic interventions against *Babesia* infection.

Keywords: Cipargamin; *Babesia* spp.; drug resistance; mutation; ATP4

Introduction

Babesia is an apicomplexan tick-transmitted hemoparasite, which not only impacts the livestock economy but also causes an emerging disease in humans (Jalovecka et al., 2019). *Babesia* is a global pathogen that is more prevalent in certain regions such as Asia, Europe, and North America. However, as climate change brings with it higher temperatures and humidity, ticks and their reservoir hosts are anticipated to expand northward for survival and activity (Drews et al., 2023). The disease it causes is known as babesiosis, commonly characterized by fever and hemolytic anemia, but chronic infections are asymptomatic (Almazán et al., 2022). In acute cases, up to 20% of patients die, particularly individuals with compromised immune systems (Krause, 2019).

Currently, the most common drugs for the treatment of human babesiosis include a combination of atovaquone (ATQ) plus azithromycin (AZM) or clindamycin plus quinine (Holbrook et al., 2023). Still, these recommended treatments often result in various problems. For instance, multiple mutations in the *B. microti* cytochrome b, which was associated with the atovaquone-target region, were discovered in an atovaquone-treated relapse patient (Holbrook et al., 2023). The combination of clindamycin and quinine is the last resort for patients with severe symptoms. Despite its efficacy, some had adverse drug reactions after taking these drugs (Vannier and Krause, 2012). The 8-aminoquinoline analog, tafenoquine (TAF), was found to be effective in curing the patient's *B. microti* infection that was resistant to azithromycin and atovaquone with a 200 mg weekly dose (Marcos et al., 2022). However, the efficacy of TAF treatment may vary between individuals and cases and its contraindication in G6PD-deficient patients limits its clinical use. Due to the aforementioned issues, it is undoubtedly urgent to search for compounds that treat infections caused by *Babesia* spp. while simultaneously minimizing the detrimental effects of antibabesial drugs.

Spiroindolone cipargamin (CIP), a promising antimalarial, has been found to effectively

74 suppress the growth of all strains of *Plasmodium falciparum* and *P. vivax* with potency in the
75 low nanomolar ranges (Rosling et al., 2018; Rottmann et al., 2010). The assessment of the
76 pharmacokinetic characteristics of the drug indicated that oral administration of CIP had good
77 absorption, a prolonged half-life, and exceptional bioavailability (Schmitt et al., 2022).
78 Following oral CIP treatment (30 mg daily for three days) in adults with simple *P. falciparum*
79 or *P. vivax* malaria, the parasitemia was rapidly cleared in a phase II trial (Schmitt et al., 2022).
80 Currently, a clinical trial is being conducted for the intravenous administration of CIP as a
81 treatment for severe malaria patients (ClinicalTrials, 2024). CIP was also evaluated for treating
82 toxoplasmosis as a second-line medicine in cases where there are intolerable toxicity issues or
83 allergies to the currently used treatments. Five days post-*Toxoplasma gondii* infection, CIP-
84 treated mice (100 mg/kg/day on the day of and the day after infection) had 90% fewer parasites
85 than the control mice (Zhou et al., 2014).

86 Due to its excellent efficacy against other apicomplexan parasites, we hypothesize that CIP
87 may also be effective as an antibabesial drug. Therefore, the objectives of this study were to
88 determine whether CIP could inhibit the growth of *Babesia* spp., namely *B. bovis* and *B. gibsoni*
89 *in vitro* and *B. microti* and *B. rodhaini in vivo*, and identify the inhibitory mechanisms of CIP
90 on *Babesia* parasites (*Bg*ATP4) by monitoring the Na^+ and H^+ balance.

91

92 **Results**

93 **Inhibitory efficacy of CIP on *B. bovis* and *B. gibsoni in vitro***

94 The *in vitro* activity of CIP against *B. bovis* and *B. gibsoni* showed a steep growth inhibition
95 curve with half inhibitory concentration (IC_{50}) values of 20.2 ± 1.4 nM (Figure 1A) and 69.4 ±
96 2.2 nM (Figure 1B), respectively. The CC_{50} value of CIP on MDCK cells was 38.7 ± 2.0 μM
97 (Figure supplement 1), resulting in a predicted selectivity index of 557.6. Furthermore, at a
98 concentration of 100 μM, CIP exhibited a low erythrocyte hemolysis rate of 0.11 ± 0.03 % (not

99 shown).

100 **CIP effect on *B. microti* and *B. rodhaini* infections *in vivo***

101 Concurrently, CIP showed effective inhibition on *B. microti* and *B. rodhaini in vivo*. The
102 parasitemia of *B. microti*-infected BALB/c mice grew dramatically in the vehicle-treated
103 control group and peaked at 10 DPI (35.88 ± 4.32%) (Figure 1C). On the other hand, the
104 treatment with CIP (20 mg/kg of body weight) or atovaquone (ATO) plus azithromycin (AZI)
105 administered orally resulted in a significantly lower peak parasitemia, 1.06 ± 0.20% and 1.61
106 ± 0.20%, respectively. Hematocrit (HCT) variations were tracked every 4 days as an indicator
107 of anemia in *B. microti*-infected mice. The vehicle-treated group showed a drop in HCT levels
108 from 8 DPI to 24 DPI, with statistically significant decreases at 12 and 16 DPI ($P < 0.01$). No
109 significant reduction in HCT levels was observed in the CIP-treated group or the ATO plus
110 AZI-treated group (Figure 1D). This suggests that the administration of CIP could control *B.*
111 *microti* infection and prevent anemia from developing in *B. microti*-infected mice. BALB/c
112 mice infected with *B. rodhaini* treated with sesame oil or ATO plus AZI showed high
113 parasitemia, 90.73 ± 1.97%, and 86.23 ± 3.06%, respectively (Figure 1E), and all mice died
114 within 10 DPI (Figure 1F). CIP treatment in *B. rodhaini*-infected mice precluded the emergence
115 of parasitemia for the following eight days (Figure 1E), which led to 66.67% of mice surviving
116 the challenge infection (Figure 1F). At 14 DPI, parasites had recurred in all CIP-treated *B.*
117 *rodhaini*-infected mice (10.32 ± 15.51%), which were eventually cleared as indicated by
118 undetectable parasites at 18 DPI (Figure 1E).

119 **Identification of *B. gibsoni* ATP4 mutation in CIP-resistant strains**

120 We sequenced the *B. gibsoni* ATP4 gene from two resistant parasite wells. A single nucleotide
121 variant (SNV) in *Bg*ATP4 with a substitution at position 2,761 (from C to G) was found − a
122 nonsynonymous coding change from leucine to valine (L921V) (Figure 2B). In another
123 resistant strain, the mutation showed in the same position. However, the nucleotide substitution

124 was from C to A, and the coding changed from leucine to isoleucine (L921I) (Figure 2C).
125 *Bg*ATP4^{L921V} and *Bg*ATP4^{L921I} lines were tested for their susceptibility to CIP, and had IC_{50}
126 values of 421.0 ± 15.88 nM and 887.9 ± 61.97 nM, respectively (Figure 2D). These findings
127 demonstrate a 6.1- and 12.8-fold reduction in CIP sensitivity of resistant parasite lines
128 *Bg*ATP4^{L921V} and *Bg*ATP4^{L921I}.

129 **The effect of CIP on *Bg*ATP4^{WT}, *Bg*ATP4^{L921V} and *Bg*ATP4^{L921I} function**

130 Microscopic observation of thin blood smears was performed to determine the morphological
131 changes of *B. gibsoni* exposed to CIP. The CIP-treated parasites became swollen after
132 incubation with the drug for 72 hr (Figure 3A). For both the treatment and control groups, one
133 hundred parasites were measured. The mean size of treated parasites was notably bigger than
134 the parasites in the untreated group ($P < 0.0001$) (Figure 3B). The addition of the ATP4
135 inhibitor CIP resulted in a time-dependent increase in the concentrations of $[Na^+]_i$ in wild-type
136 *B. gibsoni* (Figure 3C), with improved signal-to-noise ratios at the higher drug concentration
137 of 20 nM. We observed that the Na^+ concentrations in both *Bg*ATP4^{L921V} and *Bg*ATP4^{L921I} lines
138 decreased compared to those of the control *Bg*ATP4^{WT} line after being exposed to 20 nM CIP
139 for 20 min, with a significantly lower Na^+ concentration in *Bg*ATP4^{L921I} ($P = 0.0087$) (Figure
140 3E). We also demonstrated here that the addition of CIP in wild-type *B. gibsoni* caused an
141 increase in the cytosolic pH (Figure 3D). Specifically, 4 min after the drug was added, the
142 average pH of 20 nM CIP group reached as high as 7.278, while the 1 nM CIP group reached
143 7.089 and the untreated group reached 7.062. The pH values of the 20 nM CIP group were
144 consistently higher than those of the other two groups, although declining with time. In resistant
145 lines, a 20-min exposure to 20 nM CIP caused small changes in the pH values compared to the
146 wild-type line (Figure 3F), with the *Bg*ATP4^{L921I} line (7.048 ± 0.042) having a notably lower
147 pH value ($P = 0.0229$).

148 **Multiple sequence alignment of *Babesia* ATP4 and molecular docking**

149 The whole amino acid sequence of *Bg*ATP4 (GenBank: KAK1443404.1) shared identity values
150 of 29.75%, 49.40%, 49.67%, 62.21%, and 52.47% with *Homo sapiens* ATP4 (GenBank:
151 NM_000704.3), *P. falciparum* ATP4 (GenBank: PF3D7_1211900), *T. gondii* ATP4 (GenBank:
152 XP_018635122.1), *B. bovis* ATP4 (PiroplasmaDB: BBOV_IV010020), and *B. microti* ATP4
153 (GenBank: BMR1_03g01005), respectively (Figure supplement 2).
154 The pLDDT value of *Bg*ATP4^{WT} prediction was 80.7 using Colab-fold. Multiple potential
155 binding sites for CIP were revealed by blind docking throughout the whole protein surface
156 (Figure supplement 3). CIP binds in close proximity to L921, as demonstrated by focused
157 docking on this area (Figure 4A). The contribution of each residue to the predicted binding
158 affinity in either mutant structure was reduced; the precise values of *Bg*ATP4^{WT} (Figure 4B),
159 *Bg*ATP4^{L921V} (Figure 4C) and *Bg*ATP4^{L921I} (Figure 4D) were -6.43, -6.40 and -6.26 kcal/mol,
160 respectively. The interactions of CIP from each docking simulation are shown in Table
161 supplement 2.
162
163 **Discussion**
164 The repositioning of antimalarial drugs is critical in developing novel strategies for treating
165 babesiosis. CIP is a novel compound that inhibits *Plasmodium* development and has been
166 extensively tested in Phase 1 and Phase 2 clinical trials by targeting *Pf*ATP4 (Qiu et al., 2022).
167 Therefore, our study aimed to repurpose the antimalarial CIP by assessing its efficacy on
168 *Babesia* species. The IC_{50} values of CIP against *B. bovis* and *B. gibsoni in vitro* were lower
169 than the previously reported IC_{50} value of TAF (Ji et al., 2022b) and ATO against *B. gibsoni*
170 (Matsuu et al., 2004). The present investigation also demonstrated that the inhibitory effects of
171 CIP on *B. microti*-infected BALB/c mice were comparable to that of ATO plus AZI, the
172 medication prescribed by the U.S. CDC. CIP was also proven to protect mice from the deadly
173 *B. rodhaini* infection, with protection limited to 66.67% as recorded in the current trial. These

174 results suggest that CIP may be a potential chemotherapy candidate for babesiosis.

175 In a previous study, the *P. falciparum* Dd2 parent line initially had a subnanomolar IC_{50} value,
176 after the CIP-selected cultures to limiting dilution and selected clonal lines, the highly resistant
177 strain reported IC_{50} values 4200-4280 fold higher than those of wild-type Dd2 parasites with a
178 G358S mutation in the *Pf*ATP4 protein, a *P. falciparum* P-type Na^+ ATPase (Qiu et al., 2022).
179 The vital protein ATP4 is found in the parasite plasma membrane and is distinctive to the
180 subclass of the apicomplexan parasite (Mohring et al., 2022). To date, *in vitro* evolution
181 experiments using CIP have produced at least 18 parasite lines with various *Pf*ATP4 mutations
182 (Lee and Fidock, 2016; Rottmann et al., 2010). Another finding showed that the ATP4 activity
183 associated with *Tg*ATP4^{G419S} was 34 times less susceptible to CIP than that of *Tg*ATP4^{WT} (Qiu
184 et al., 2022). It follows that there is a significant chance that the resistant *Babesia* parasites will
185 also emerge from CIP exposure. In this study, we successfully produced two CIP-resistant
186 strains using six independent selections. The newly discovered L921V and L921I mutations in
187 *Bg*ATP4 decreased the CIP sensitivity by 6.1 and 12.8 times, respectively. We provided
188 compelling evidence that natural variety mutations L921V and L921I in *Bg*ATP4 significantly
189 affected the proteins' susceptibility to CIP inhibition, albeit the mutational sites were different
190 from those of *P. falciparum* and *T. gondii*.

191 Although ATP4 was initially recognized as a Ca^{2+} transporter (Krishna et al., 2001), current
192 evidence suggests that ATP4 functions as an ATPase for exporting Na^+ while importing H^+
193 (Mohring et al., 2022), as well as causing a variety of other physiological perturbations
194 including an increase in the volume of parasites and infected erythrocytes, due to the osmotic
195 impact of the $[Na^+]_{cyt}$ increase (Dennis et al., 2018), a decline in cholesterol extrusion from the
196 parasite plasma membrane as a result of the increase in $[Na^+]_{cyt}$ (Das et al., 2016), and an
197 intensified rigidity of erythrocytes infected with ring-stage parasites (Zhang et al., 2016). In
198 this study, the CIP-exposed wild-type *B. gibsoni* became swollen, which was identical to a prior

199 study on *P. falciparum* (Dennis et al., 2018). We hypothesize that the swelling of the isolated
200 parasites can be ascribed to the osmotic consequences of Na^+ uptake and is contingent upon
201 the presence of Na^+ in the external environment. This hypothesis is supported by the following
202 experimental results.

203 The output of Na^+ and input of H^+ diminished upon CIP-induced inhibition of *Pf*ATP4, and
204 the continued outflow of H^+ via V-type H^+-ATPase led to an alkalinization that ultimately killed
205 the parasites (Spillman et al., 2013). Our capacity to measure a time-dependent increase in the
206 concentration of $[Na^+]_i$ and pH value for wild-type *B. gibsoni* facilitated us to gain insight into
207 the basic mechanisms of CIP on *Bg*ATP4^{WT} function. Furthermore, our results validate that
208 internal alkalinization was the main factor in *Babesia* death and support our hypothesis that the
209 swollen isolated parasites were produced by Na^+ absorption. To explore further how mutations
210 in *Bg*ATP4 are associated with the upregulation of the parasite's $[Na^+]_i$ and $[H^+]_i$, we tested two
211 *Bg*ATP4-mutant lines that were chosen previously with *Bg*ATP4 inhibitors (*Bg*ATP4^{L921V} and
212 *Bg*ATP4^{L921I}). Due to the presence of L921V and L921I mutations in drug-resistant strains of
213 *Bg*ATP4, the concentration of Na^+ did not increase as much as it would have in the wild-type
214 strain following the addition of 20 nM CIP for 20 min. As intraerythrocytic alkalinization rises,
215 the same outcome happens. From these results, we deduced how natural mutations in *Bg*ATP4
216 may affect ATP4 inhibitor susceptibility by dysregulating H^+ and Na^+ balance, which helped
217 parasites survive in a relatively high concentration of CIP. An illustration of the putative
218 processes for regulating Na^+ and H^+ in erythrocytes infected with the *Babesia* parasite is
219 presented in Figure supplement 4.

220 According to studies using the *Pf*ATP4 model for molecular docking, the G358S mutation
221 results in a steric clash that lowers CIP's binding affinity (Qiu et al., 2022). The results from
222 the current study were similar to the *Pf*ATP4 model. The molecular docking was constructed
223 using a ColabFold model of wild-type *Bg*ATP4, which predicted the binding mode and affinity
224 between ATP4 protein and the ligand to provide a possible mechanistic explanation. It
225 suggested that the L921V mutation caused changes at the atomic level, whereas the L921I
226 mutation created a steric clash that reduced the binding affinity of CIP. The predicted affinity
227 score of the L921I mutation was lower than that of the L921V mutation. Thus, it is possible

228 that *Bg*ATP4^{L921I} has a weaker binding to the drug compared to *Bg*ATP4^{L921V}. These findings
229 are consistent with the results obtained from measuring the IC_{50} of the drug against parasites
230 with the L921V and L921I mutations.
231
232 **Materials and methods**
233 **Parasite culture**
234 The parasites *B. gibsoni* (Oita strain) and *B. bovis* Texas strain were *in vitro* cultured in 24-well
235 plates and maintained in an atmosphere of 5% CO_2 and 5% O_2 at 37 °C (Liu et al., 2018). For
236 the *in vivo* studies, *B. microti* Peabody mjr strain-(ATCC PRA-99) and *B. rodhaini* Australia
237 strain-infected RBCs (iRBCs), which were collected and diluted with phosphate-buffered
238 saline (PBS) when the parasitemia levels in the donor mice reached ~20% and 50%,
239 respectively, and were intraperitoneally injected into BALB/c mice. Each BALB/c mouse was
240 infected with 1.0×10^7 *B. microti* or *B. rodhaini* iRBCs for the *in vivo* trials (Ji et al., 2022a).
241 ***In vitro* cytotoxicity of CIP in canine cells and hemolysis rate in canine erythrocytes**
242 Cultures of Madin-Darby canine kidney (MDCK) cells were maintained at 37 °C under an
243 atmosphere of 5% CO_2 and 5% O_2 and the cytotoxic effect of CIP (MedChem Express, Tokyo,
244 Japan) was assessed using a cell viability assay by CCK-8 (Dojindo, Japan) as described
245 previously (Li et al., 2023). The selectivity index is calculated as the ratio between the half
246 maximal inhibitory concentration (IC_{50}) and the 50% cytotoxic concentration (CC_{50}) values.
247 Canine erythrocytes were collected from healthy beagle dogs raised in NRCPD and stocked in
248 Vega y Martinez (VYM) phosphate-buffered saline solution at 4 °C (Vega et al., 1985). A
249 canine erythrocyte hemolysis assay was performed at concentrations of 0.1, 1, 5, 10, 25, 50,
250 and 100 μM as previously described (Ariefta et al., 2022).
251 **Evaluation of the efficacy of CIP against *Babesia* parasites *in vitro***
252 The efficacy of CIP against *B. gibsoni* and *B. bovis* was determined using a fluorescence assay,

253 as previously described (Guswanto et al., 2014). The IC_{50} values were determined from the
254 fluorescence values and by non-linear regression analysis (curve fit) in GraphPad Prism 9
255 (GraphPad Software Inc., USA).

256 **Chemotherapeutic effects of CIP against *Babesia* infections *in vivo***

257 CIP was evaluated on *B. microti*- and *B. rodhaini*-infected mice, as previously described
258 (Ndayisaba et al., 2021; Tuvshintulga et al., 2022). When all mice had a 1% average parasitemia
259 at 4 days postinfection (DPI), the drug treatments were administered, which continued for
260 seven days. Three groups of *B. microti*-infected mice were administered different treatments.
261 The CIP group (n = 6) and the ATO plus AZI group (n = 6) were orally treated with 20 mg/kg
262 CIP and 20 mg/kg ATO plus AZI (Sigma, Tokyo, Japan), respectively. The infected mice of the
263 vehicle group (n = 6) orally received 0.2 mL of sesame oil as the control. Eighteen mice infected
264 with *B. rodhaini* were likewise placed into three groups for treatment, and they received the
265 same care as the mice infected with *B. microti*. A light microscope (Nikon, Japan) and a
266 hematology analyzer (Celltac α MEK-6450, Nihon Kohden Corporation, Tokyo, Japan) were
267 used to observe the parasitemia and hematocrit levels every two and four days, respectively.

268 **Selection of CIP-resistant *B. gibsoni in vitro***

269 Selections were initiated by exposing six independent flasks, each containing 10 μL *B. gibsoni*
270 iRBCs mixed with 40 μL RBC into a 450 μL culture medium, which contained increasing
271 concentrations of CIP: 5, 10, 20, 30 to 694 nM ($10\times IC_{50}$). The medium containing CIP was
272 replaced daily until parasites treated with $10\times IC_{50}$ CIP reached multiplication rates that were
273 approximately comparable to those of the untreated controls (Hwang et al., 2010). Then, to
274 evaluate the decreased sensitivity to CIP, IC_{50} values of resistant strains were determined by
275 nonlinear regression using the GraphPad Prism software.

276 **Detection of *B. gibsoni* ATP4 gene mutations**

277 The genomic DNA of the mutant parasites was extracted and sequenced (Ji et al., 2022a). The

278 primer sets used for sequencing are listed in Table supplement 1. The single nucleotide variants
279 were confirmed by pairwise alignment to the *Bg*ATP4^{WT} sequence (GenBank:
280 JAVEPI010000002.1).

281 **Morphological changes in CIP-treated *in vitro* cultured *B. gibsoni***

282 A microscopy assay was used to detect the morphological changes of wild-type *B. gibsoni* after
283 exposure to 50 nM CIP for three consecutive days (Liu et al., 2021; Tayebwa et al., 2018). At
284 4 days post-treatment, ImageJ software was used to measure the sizes of 100 randomly selected
285 parasites in the CIP-treated group and the control group on Giemsa-stained blood smears.

286 **Parasites $[Na^+]_i$ and pH_i measurements**

287 For both $[Na^+]_i$ and pH_i measurements, the wild-type and mutant parasites were initially
288 separated from erythrocytes by treatment with saponin (0.05% [wt/vol]) for 5 min (Saliba and
289 Kirk, 1999). The Na^+-sensitive fluorescent dye SBFI (Thermo Fisher Scientific; product
290 S1263) was used to quantify intracellular sodium ($[Na^+]_i$). Saponin-isolated parasites (at 1×10^8
291 parasites/mL) were loaded with SBFI (5 μM; in the presence of 0.02% w/v Pluronic F127) for
292 1 hr at room temperature (RT) (Spillman et al., 2013). Thereafter, SBFI-loaded parasites were
293 resuspended in physiological saline (120 mM NaCl, 5 mM KCl, 25 mM HEPES, 20 mM D-
294 glucose, and 1 mM $MgCl_2$ [pH 7.1]) at RT in the presence or absence of CIP. A 96-well
295 microtiter plate was filled with around 200 μL of parasite suspension per well. The dye-loaded
296 cells fluoresced at 515 nm after being stimulated at 340 and 380 nm. Parasites loaded with
297 SBFI were suspended in calibration buffers containing $[Na^+]$ values ranging from 0 to 140 mM
298 (pH 7.1) to establish calibration curves (Diarra et al., 2001).

299 The cytosolic pH of wild-type and mutant strains was measured using the pH-sensitive
300 fluorescent dye BCECF [2',7'-bis-(2-carboxyethyl)-5-(and-6)- carboxyfluorescein] (Biotium;
301 product 51011). The BCECF was added to saponin-isolated parasites by suspension (1×10^8
302 parasites/mL) and incubated for 20 minutes at 37 °C in RPMI-1640 culture medium (Gibco,

303 USA) (Saliba and Kirk, 1999). Thereafter, the parasites loaded with dye were rinsed thrice
304 (12,000 × g, 1 min) in RPMI-1640 culture medium, then resuspended in physiological saline
305 (as previously mentioned) with or without various concentrations of CIP. A 96-well microtiter
306 plate was filled with around 200 μL of parasite suspension per well. The dye-loaded cells
307 fluoresced at 520 nm after being stimulated at 440 and 490 nm. A pH calibration was carried
308 out for each experiment (Mohring et al., 2022).

309 **Multiple ATP4 sequence alignment and molecular docking**

310 *B. gibsoni* ATP4 (GenBank: KAK1443404.1), *B. bovis* ATP4 (PiroplasmaDB:
311 BBOV_IV010020), *B. microti* ATP4 (GenBank: BMR1_03g01005), *T. gondii* ATP4
312 (GenBank: XP_018635122.1), and *Homo sapiens* ATP4 (GenBank: NM_000704.3) sequences
313 were obtained by a homology search using *P. falciparum* ATP4 (GenBank: PF3D7_1211900).
314 Sequence alignment was analyzed using MUSCLE in Jalview v2.11.3.2 software and BLAST
315 (http://www.ncbi.nlm.nih.gov/BLAST/).

316 AlphaFold was used to predict the structure of *Bg*ATP4^{WT} (Jumper et al., 2021). Using the
317 GROMACS 2021 Molecular Dynamics package, the energy minimization was carried out
318 following the model's generation (Lindahl et al., 2021). The mutations were produced by using
319 Charmm-GUI PDB reader (Jo et al., 2014). PyMol (version 2.0 Schrödinger, LLC) was used
320 to confirm the position of the mutation site (center: -20.367, 10.904, 9.435; size: 30×30×30)
321 (Trott and Olson, 2010). The ligand molecules CIP was downloaded from PubChem (CID
322 44469321 (https://pubchem.ncbi.nlm.nih.gov/compound/ 44469321). The ligand was used to
323 dock with Gnina (Eberhardt et al., 2021). The affinity score and binding pose were chosen only
324 from the highest CNN (convolutional neural network) score results from docking simulations.
325 The models were visualized using the PyMOL Molecular Graphic System and Discovery
326 Studio.

327 **Statistical analysis**

Data analysis, namely one-way analysis of variance (ANOVA) and two-tailed unpaired t-tests, was performed using GraphPad Prism (La Jolla, CA, USA) version 9. A P value of <0.05 was considered a statistically significant result.

Acknowledgments

This work was supported by a Grant-in-Aid for Scientific Research (22H02509), the JSPS Core-to-Core program, both from the Ministry of Education, Culture, Sports, Science, and Technology of Japan, and a grant from the Strategic International Collaborative Research Project (JPJ008837) promoted by the Ministry of Agriculture, Forestry, and Fisheries of Japan, and Natural Science Foundation of Hubei Province (2023AFC001).

Declaration of Competing Interest

The authors declare that they have no known competing financial interests or personal relationships that could have appeared to influence the work reported in this paper.

Author contributions

Hang Li, Investigation, Data curation, Formal analysis, Writing – original draft, Writing – review & editing; Shengwei Ji, Methodology, Investigation, Software, Validation; Nanang R. Ariefta, Methodology, Software, Formal analysis; Eloiza May S. Galon, Visualization, Writing – review & editing; Shimaa AES El-Sayed, Methodology, Visualization; Lijun Jia, Data curation, Visualization; Yoshifumi Nishikawa, Methodology, Resources; Mingming Liu, Conceptualization, Methodology, Investigation, Resources, Data curation, Funding acquisition, Supervision, Writing – review & editing; Xuenan Xuan, Conceptualization, Methodology, Validation, Formal analysis, Supervision, Project administration, Writing – review & editing.

Ethics

All animal experiments were performed according to the Guide for the Care and Use of Laboratory Animals of Obihiro University of Agriculture and Veterinary Medicine, which was also approved by the Committee on the Ethics of Animal Experiments at the Obihiro University of Agriculture and Veterinary Medicine, Japan (permit numbers: animal experiment, 22-145 and 23-132; DNA experiment, 2207 and 2208; pathogen, 202308 and 202306).

References

Almazán C, Scimeca RC, Reichard MV, Mosqueda J. 2022. Babesiosis and Theileriosis in North America. *Pathogens* **11**:168. doi:10.3390/pathogens11020168

Ariefta NR, Pagmadulam B, Nihei C, Nishikawa Y. 2022. Sparsomycin exhibits potent antiplasmodial activity *in vitro* and *in vivo*. *Pharmaceutics* **14**:544. doi:10.3390/pharmaceutics14030544

ClinicalTrials.gov [Internet]. Bethesda (MD): National Library of Medicine (US). Identifier NCT04675931, To evaluate efficacy, safety, tolerability and PK of intravenous cipargamin in participants with severe *Plasmodium falciparum* malaria; 2024 Feb 29 [cited 2024 Apr 9]. Available from: https://clinicaltrials.gov/study/NCT04675931

Das S, Bhatanagar S, Morrisey JM, Daly TM, Burns JM, Coppens I, Vaidya AB. 2016. Na^+ influx induced by new antimalarials causes rapid alterations in the cholesterol content and morphology of *Plasmodium falciparum*. *PLoS Pathog* **12**:e1005647. doi:10.1371/journal.ppat.1005647

Dennis ASM, Lehane AM, Ridgway MC, Holleran JP, Kirk K. 2018. Cell swelling induced by the antimalarial KAE609 (cipargamin) and other *Pf*ATP4-associated antimalarials. *Antimicrob Agents Chemother* **62**:e00087-18. doi:10.1128/AAC.00087-18

Diarra A, Sheldon C, Church J. 2001. In situ calibration and [H^+] sensitivity of the fluorescent Na^+ indicator SBFI. *American Journal of Physiology-Cell Physiology* **280**:C1623–C1633. doi:10.1152/ajpcell.2001.280.6.C1623

Drews SJ, Kjemtrup AM, Krause PJ, Lambert G, Leiby DA, Lewin A, O'Brien SF, Renaud C, Tonnetti L, Bloch EM. 2023. Transfusion-transmitted *Babesia* spp.: a changing landscape of epidemiology, regulation, and risk mitigation. *J Clin Microbiol* **61**:e01268-22. doi:10.1128/jcm.01268-22

Eberhardt J, Santos-Martins D, Tillack AF, Forli S. 2021. AutoDock Vina 1.2.0: new docking methods, expanded force field, and python bindings. *J Chem Inf Model* **61**:3891–3898.

doi:10.1021/acs.jcim.1c00203

Guswanto A, Sivakumar T, Rizk MA, Elsayed SAE, Youssef MA, ElSaid EES, Yokoyama N, Igarashi I. 2014. Evaluation of a fluorescence-based method for antibabesial drug screening. *Antimicrob Agents Chemother* **58**:4713–4717. doi:10.1128/AAC.00022-14

Holbrook NR, Klontz EH, Adams GC, Schnittman SR, Issa NC, Bond SA, Branda JA, Lemieux JE. 2023. *Babesia microti* variant with multiple resistance mutations detected in an immunocompromised patient receiving atovaquone prophylaxi. *Open Forum Infectious Diseases* **10**:ofad097. doi:10.1093/ofid/ofad097

Hwang S-J, Yamasaki M, Nakamura K, Sasaki N, Murakami M, Wickramasekara Rajapakshage BK, Ohta H, Maede Y, Takiguchi M. 2010. Development and characterization of a strain of *Babesia gibsoni* resistant to diminazene aceturate *in vitro*. *J Vet Med Sci* **72**:765–771. doi:10.1292/jvms.09-0535

Jalovecka M, Sojka D, Ascencio M, Schnittger L. 2019. *Babesia* life cycle-when phylogeny meets biology. *Trends in Parasitology* **35**:356–368. doi:10.1016/j.pt.2019.01.007

Ji S, Galon EM, Rizk MA, Yi Y, Zafar I, Li H, Ma Z, Iguchi A, Asada M, Liu M, Xuan X. 2022. Efficacy of the antimalarial MMV390048 against *Babesia* infection reveals phosphatidylinositol 4-kinase as a druggable target for babesiosis. *Antimicrob Agents Chemother* **66**:e00574-22. doi:10.1128/aac.00574-22

Ji S, Liu M, Galon EM, Rizk MA, Tuvshintulga B, Li J, Zafar I, Hasegawa Y, Iguchi A, Yokoyama N, Xuan X. 2022. Inhibitory effect of naphthoquine phosphate on *Babesia gibsoni in vitro* and *Babesia rodhaini in vivo*. *Parasites Vectors* **15**:10. doi:10.1186/s13071-021-05127-0

Jo S, Cheng X, Islam SM, Huang L, Rui H, Zhu A, Lee HS, Qi Y, Han W, Vanommeslaeghe K, MacKerell AD, Roux B, Im W. 2014. CHARMM-GUI PDB manipulator for advanced modeling and simulations of proteins containing nonstandard residues. *Adv Protein Chem Struct Biol* **96:** 235–265. doi:10.1016/bs.apcsb.2014.06.002

Jumper J, Evans R, Pritzel A, Green T, Figurnov M, Ronneberger O, Tunyasuvunakool K, Bates R, Žídek A, Potapenko A, Bridgland A, Meyer C, Kohl SAA, Ballard AJ, Cowie A, Romera-Paredes B, Nikolov S, Jain R, Adler J, Back T, et al. 2021. Highly accurate protein structure prediction with AlphaFold. *Nature* **596**:583–589. doi:10.1038/s41586-021-03819-2

Krause PJ. 2019. Human babesiosis. *International Journal for Parasitology* **49**:165–174. doi:10.1016/j.ijpara.2018.11.007

Krishna S, Woodrow C, Webb R, Penny J, Takeyasu K, Kimura M, East JM. 2001. Expression and functional characterization of a *Plasmodium falciparum* $Ca2^{+}$-ATPase (*Pf*ATP4) belonging to a subclass unique to apicomplexan organisms. *Journal of Biological Chemistry* **276**:10782–10787. doi:10.1074/jbc.M010554200

Lee AH, Fidock DA. 2016. Evidence of a mild mutator phenotype in cambodian *Plasmodium falciparum* malaria parasites. *PLoS ONE* **11**:e0154166. doi:10.1371/journal.pone.0154166

424 Li H, Galon EM, Ji S, Zafar I, Ma Z, Do T, Amer MM, Ma Y, Liu M, Xuan X. 2023. *In vitro*
425 screening of compounds from the Food and Drug Administration-approved library identifies
426 anti-*Babesia gibsoni* activity of idarubicin hydrochloride and vorinostat. *Parasitology*
427 *International* **96**:102774. doi:10.1016/j.parint.2023.102774
428 Lindahl, Abraham, Hess, Spoel VD. 2021. GROMACS 2021 Manual.
429 doi:10.5281/ZENODO.4457591
430 Liu M, Adjou Moumouni PF, Cao S, Asada M, Wang G, Gao Y, Guo H, Li J, Vudriko P,
431 Efstratiou A, Ringo AE, Lee S-H, Hakimi H, Masatani T, Sunaga F, Kawazu S, Yamagishi J,
432 Jia L, Inoue N, Xuan X. 2018. Identification and characterization of interchangeable cross-
433 species functional promoters between *Babesia gibsoni* and *Babesia bovis*. *Ticks and Tick-*
434 *borne Diseases* **9**:330–333. doi:10.1016/j.ttbdis.2017.11.008
435 Liu M, Ji S, Kondoh D, Galon EM, Li J, Tomihari M, Yanagawa M, Tagawa M, Adachi M,
436 Asada M, Igarashi I, Iguchi A, Xuan X. 2021. Tafenoquine is a promising drug candidate for
437 the treatment of babesiosis. *Antimicrob Agents Chemother* **65**:e00204-21.
438 doi:10.1128/AAC.00204-21
439 Marcos LA, Leung A, Kirkman L, Wormser GP. 2022. Use of tafenoquine to treat a patient
440 with relapsing babesiosis with clinical and molecular evidence of resistance to azithromycin
441 and atovaquone. *IDCases* **27**:e01460. doi:10.1016/j.idcr.2022.e01460
442 Matsuu A, Koshida Y, Kawahara M, Inoue K, Ikadai H, Hikasa Y, Okano S, Higuchi S. 2004.
443 Efficacy of atovaquone against *Babesia gibsoni in vivo* and *in vitro*. *Veterinary Parasitology*
444 **124**:9–18. doi:10.1016/j.vetpar.2004.07.005
445 Mohring F, Van Schalkwyk DA, Henrici RC, Blasco B, Leroy D, Sutherland CJ, Moon RW.
446 2022. Cation ATPase (ATP4) orthologue replacement in the malaria parasite *Plasmodium*
447 *knowlesi* reveals species-specific responses to ATP4-targeting drugs. *mBio* **13**:e01178-22.
448 doi:10.1128/mbio.01178-22
449 Ndayisaba G, Yeka A, Asante KP, Grobusch MP, Karita E, Mugerwa H, Asiimwe S, Oduro A,
450 Fofana B, Doumbia S, Jain JP, Barsainya S, Kullak-Ublick GA, Su G, Schmitt EK, Csermak
451 K, Gandhi P, Hughes D. 2021. Hepatic safety and tolerability of cipargamin (KAE609), in
452 adult patients with *Plasmodium falciparum* malaria: a randomized, phase II, controlled,
453 dose-escalation trial in sub-Saharan Africa. *Malar J* **20**:478. doi:10.1186/s12936-021-
454 04009-1
455 Qiu D, Pei JV, Rosling JEO, Thathy V, Li D, Xue Y, Tanner JD, Penington JS, Aw YTV, Aw
456 JYH, Xu G, Tripathi AK, Gnadig NF, Yeo T, Fairhurst KJ, Stokes BH, Murithi JM,
457 Kümpornsin K, Hasemer H, Dennis ASM, et al. 2022. A G358S mutation in the *Plasmodium*
458 *falciparum* Na^+ pump *Pf*ATP4 confers clinically-relevant resistance to cipargamin. *Nat*
459 *Commun* **13**:5746. doi:10.1038/s41467-022-33403-9
460 Rosling JEO, Ridgway MC, Summers RL, Kirk K, Lehane AM. 2018. Biochemical
461 characterization and chemical inhibition of *Pf*ATP4-associated Na^+-ATPase activity in

462 *Plasmodium falciparum* membranes. *Journal of Biological Chemistry* **293**:13327–13337.
463 doi:10.1074/jbc.RA118.003640
464 Rottmann M, McNamara C, Yeung BKS, Lee MCS, Zou B, Russell B, Seitz P, Plouffe DM,
465 Dharia NV, Tan J, Cohen SB, Spencer KR, González-Páez GE, Lakshminarayana SB, Goh
466 A, Suwanarusk R, Jegla T, Schmitt EK, Beck H-P, Brun R, et al. 2010. Spiroindolones, a
467 potent compound class for the treatment of malaria. *Science* **329**:1175–1180.
468 doi:10.1126/science.1193225
469 Saliba KJ, Kirk K. 1999. pH regulation in the intracellular malaria parasite, *Plasmodium*
470 *falciparum*. *Journal of Biological Chemistry* **274**:33213–33219.
471 doi:10.1074/jbc.274.47.33213
472 Schmitt EK, Ndayisaba G, Yeka A, Asante KP, Grobusch MP, Karita E, Mugerwa H, Asiimwe
473 S, Oduro A, Fofana B, Doumbia S, Su G, Csermak Renner K, Venishetty VK, Sayyed S,
474 Straimer J, Demin I, Barsainya S, Boulton C, Gandhi P. 2022. Efficacy of cipargamin
475 (KAE609) in a randomized, phase II dose-escalation study in adults in Sub-Saharan Africa
476 with uncomplicated *Plasmodium falciparum* malaria. *Clinical Infectious Diseases* **74**:1831–
477 1839. doi:10.1093/cid/ciab716
478 Spillman NJ, Allen RJW, McNamara CW, Yeung BKS, Winzeler EA, Diagana TT, Kirk K.
479 2013. Na^+ regulation in the malaria parasite *Plasmodium falciparum* involves the cation
480 ATPase *Pf*ATP4 and is a target of the spiroindolone antimalarials. *Cell Host & Microbe*
481 **13**:227–237. doi:10.1016/j.chom.2012.12.006
482 Tayebwa DS, Tuvshintulga B, Guswanto A, Nugraha AB, Batiha GE-S, Gantuya S, Rizk MA,
483 Vudriko P, Sivakumar T, Yokoyama N, Igarashi I. 2018. The effects of nitidine chloride and
484 camptothecin on the growth of *Babesia* and *Theileria* parasites. *Ticks and Tick-borne*
485 *Diseases* **9**:1192–1201. doi:10.1016/j.ttbdis.2018.04.019
486 Trott O, Olson AJ. 2010. AutoDock Vina: improving the speed and accuracy of docking with a
487 new scoring function, efficient optimization, and multithreading. *J Comput Chem* **31**:455–
488 461. doi:10.1002/jcc.21334
489 Tuvshintulga B, Sivakumar T, Nugraha AB, Ahedor B, Batmagnai E, Otgonsuren D, Liu M,
490 Xuan X, Igarashi I, Yokoyama N. 2022. Combination of clofazimine and atovaquone as a
491 potent therapeutic regimen for the radical cure of *Babesia microti* infection in
492 immunocompromised hosts. *The Journal of Infectious Diseases* **225**:238–242.
493 doi:10.1093/infdis/jiab537
494 Vannier E, Krause PJ. 2012. Human Babesiosis. *N Engl J Med* **366**:2397–2407.
495 doi:10.1056/NEJMra1202018
496 Vega CA, Buening GM, Green TJ, Carson CA. 1985. *In vitro* cultivation of *Babesia bigemina*.
497 *Am J Vet Res* **46**:416–420.
498 Zhang R, Suwanarusk R, Malleret B, Cooke BM, Nosten F, Lau Y-L, Dao M, Lim CT, Renia
499 L, Tan KSW, Russell B. 2016. A basis for rapid clearance of circulating ring-stage malaria

500 parasites by the spiroindolone KAE609. *J Infect Dis* **213**:100–104. doi:10.1093/infdis/jiv358
501 Zhou Y, Fomovska A, Muench S, Lai B-S, Mui E, McLeod R. 2014. Spiroindolone that inhibits
502 *Pf*ATPase4 is a potent, cidal inhibitor of *Toxoplasma gondii* tachyzoites *in vitro* and *in vivo*.
503 *Antimicrob Agents Chemother* **58**:1789–1792. doi:10.1128/AAC.02225-13
504

505

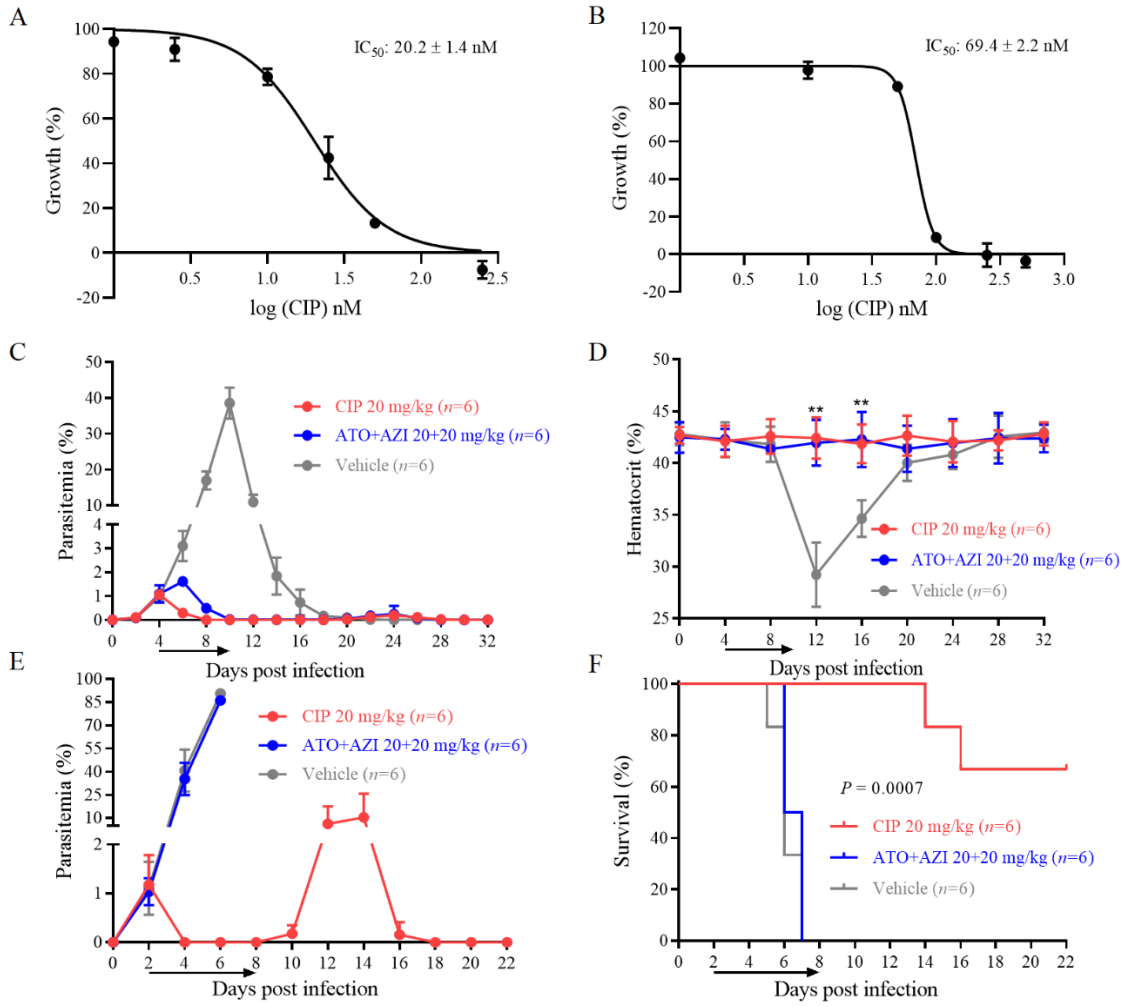

506

507 **Figure 1. CIP demonstrates potent inhibition on *Babesia* spp.. (A)** and **(B)** Dose-dependent
508 growth curve of CIP on *B. bovis* and *B. gibsoni in vitro*. Each value represents the mean ±
509 standard deviation (SD) of three independent experiments carried out in triplicate. **(C)**
510 Inhibitory effects of CIP and atovaquone (ATO) plus azithromycin (AZI) on the proliferation
511 of *B. microti* in BALB/c mice. **(D)** Hematocrit (HCT) values in mice treated with CIP or ATO
512 plus AZI compared with vehicle-treated mice. **(E)** Inhibitory effects of CIP and atovaquone
513 (ATO) plus azithromycin (AZI) on the proliferation of *B. rodhaini* in BALB/c mice. **(F)**
514 Survival rates of CIP-treated, ATO plus AZI-treated, and vehicle-treated mice. The treatment
515 time is shown by arrows, and significant differences ($P < 0.01$) between the drug-treated groups
516 and the vehicle-treated control group are indicated by asterisks. The data from one of six
517 individual experiments are expressed as means ± SD. *, $P < 0.05$; **, $P < 0.01$.

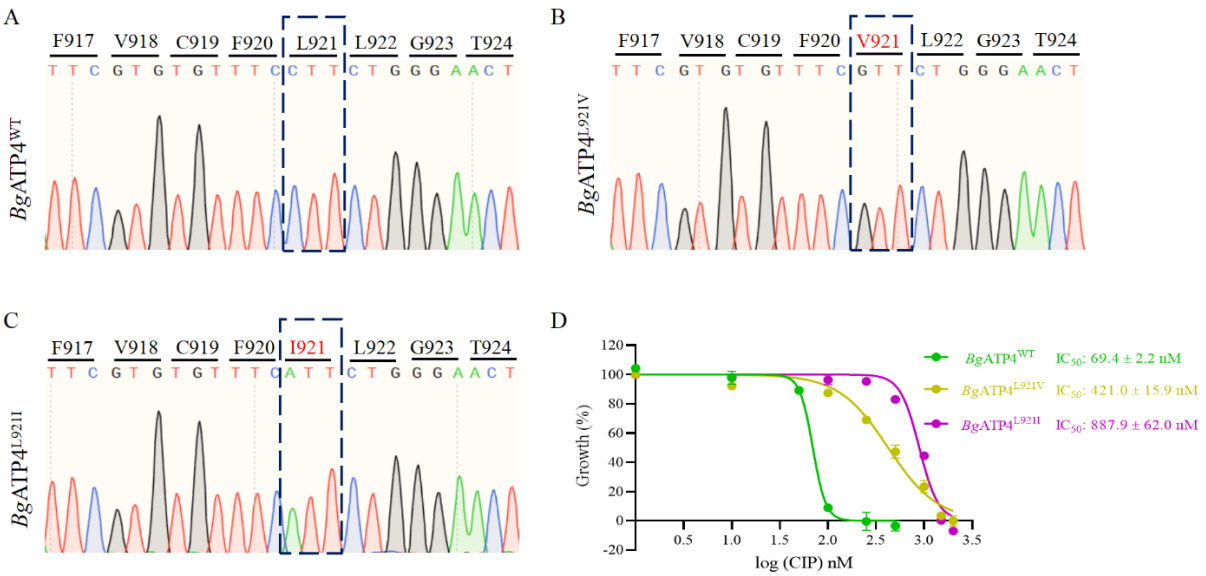

518

519 **Figure 2. Mutations in *Bg*ATP4 mediate CIP resistance. (A-C)** Representative sequencing
520 chromatogram of resistant parasites from CIP-treated *B. gibsoni*. The resistant parasite genomic
521 DNA is extracted from blood samples after a 60 day-treatment. The *Bg*ATP4 gene was
522 amplified and sequenced using the DNA. **(D)** Dose-dependent growth curve of *Bg*ATP4^{WT},
523 *Bg*ATP4^{L921V}, and *Bg*ATP4^{L921I} *in vitro*. Each value represents the mean ± standard deviation
524 (SD) of three independent experiments carried out in triplicate.

525

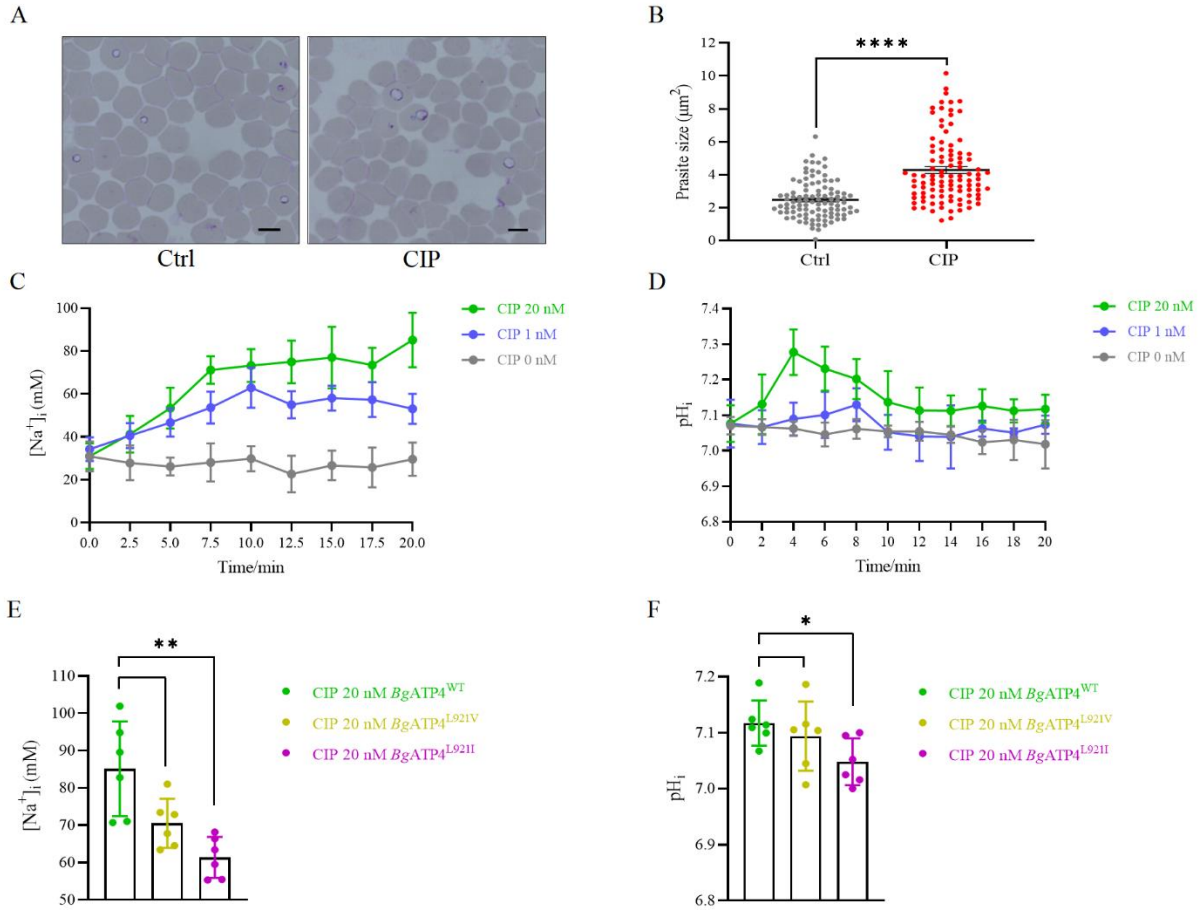

Figure 3. Effect of CIP on $[Na^+]_i$ and pH regulation in *B. gibsoni* lines. (A) Untreated and CIP-treated parasite morphology after incubation for 72 h. Scale bar: 5 μm. (**B**) Sizes of 100 parasites in two groups measured with ImageJ software in panels A. Statistically significant differences between the means of variables determined by t-test. ****, $P < 0.0001$. (**C**) $[Na^+]_i$ concentrations after addition of CIP in *Bg*ATP4^{WT} line. Representative traces from the experiment that highlight the impact of adding 20 nM CIP (green), 1 nM CIP (blue), or 0 nM CIP (grey) on the concentration $[Na^+]_i$ of the *Bg*ATP4^{WT} line. (**D**) Alkalinization of pH_i in *Bg*ATP4^{WT} line upon addition of the ATP4 inhibitor. (**E**) Addition of 20 nM CIP to the wild-type and resistant parasite lines results in different $[Na^+]_i$ concentrations. (**F**) Addition of 20 nM CIP to the wild-type and resistant parasite lines results in different pH_i concentrations. Experiments were performed in technical duplicates for at least three biological repeats. ns, non significant, $p > 0.05$; *, $P < 0.05$; **, $P < 0.01$.

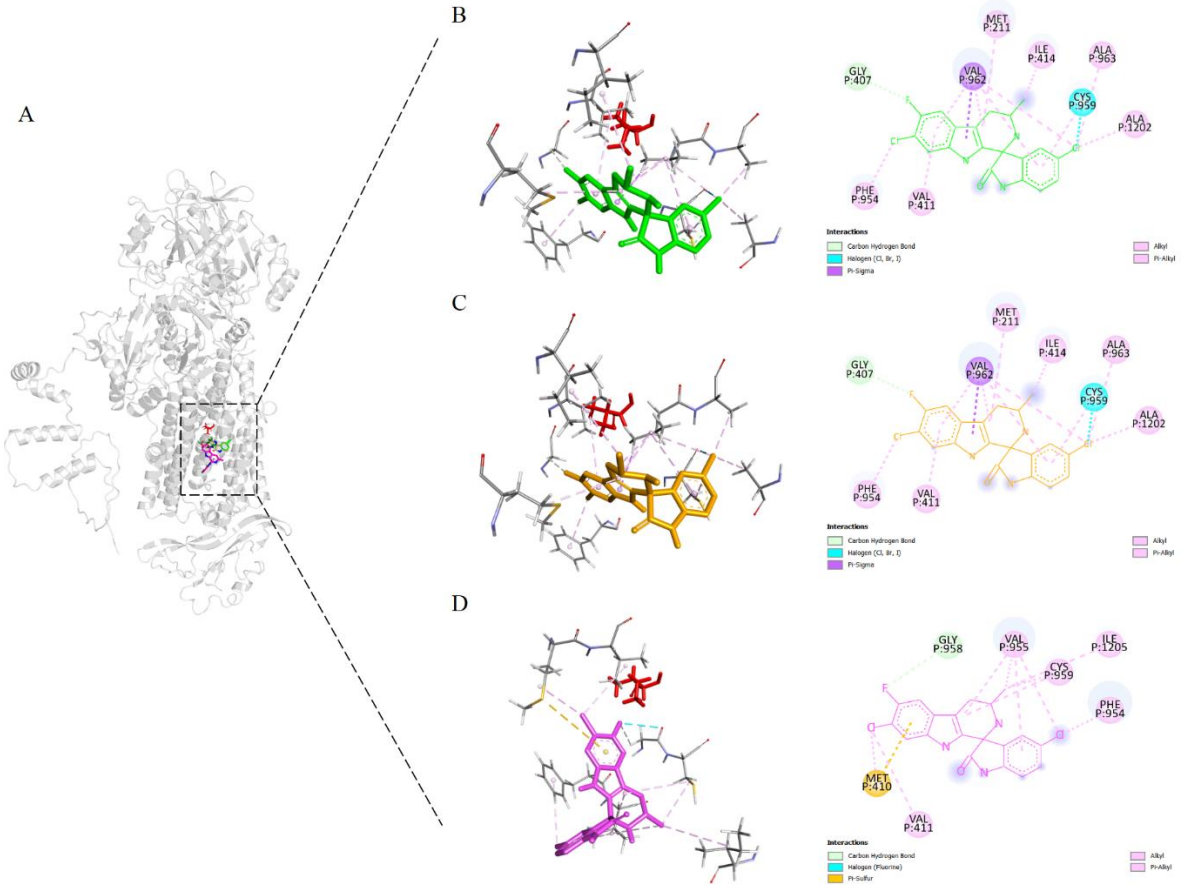

539

540 **Figure 4. Binding sites proximal to *Bg*ATP4 residue 921 predicted by molecular docking.**

541 **(A)** The lowest energy poses for CIP were located in reference to the whole protein structure,

542 docking against the WT (green), L921V (yellow), and L921I (pink) mutant *Bg*ATP4. The side

543 chain of L921 is also shown in a red stick at its position. (**B-D)** The zoomed views of the

544 binding locations of CIP.

545

546 ***Supplementary Material***

547

548 **Supplementary Figures**

549

550

551

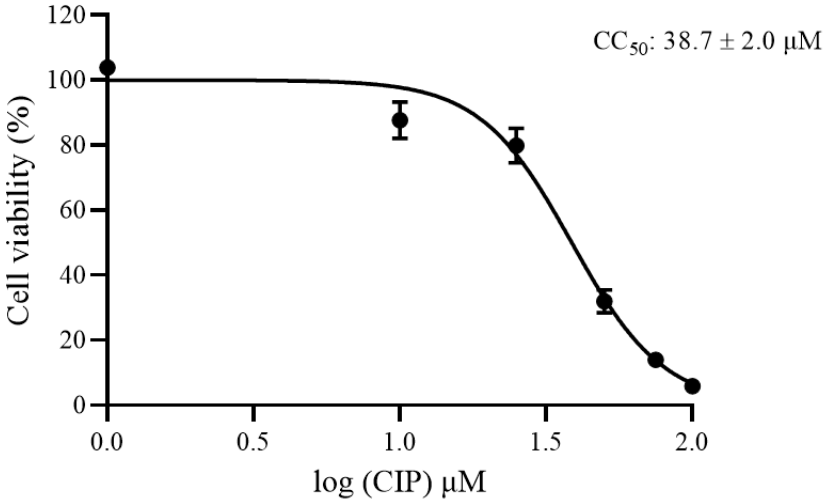

552

553 **Figure supplement 1. Cytotoxicity assay of CIP on the MDCK cell line.** The MTP-500

554 microplate reader is utilized to detect the absorbance at 450 nm. The results are displayed as

555 the mean ± standard deviation of three separate tests.

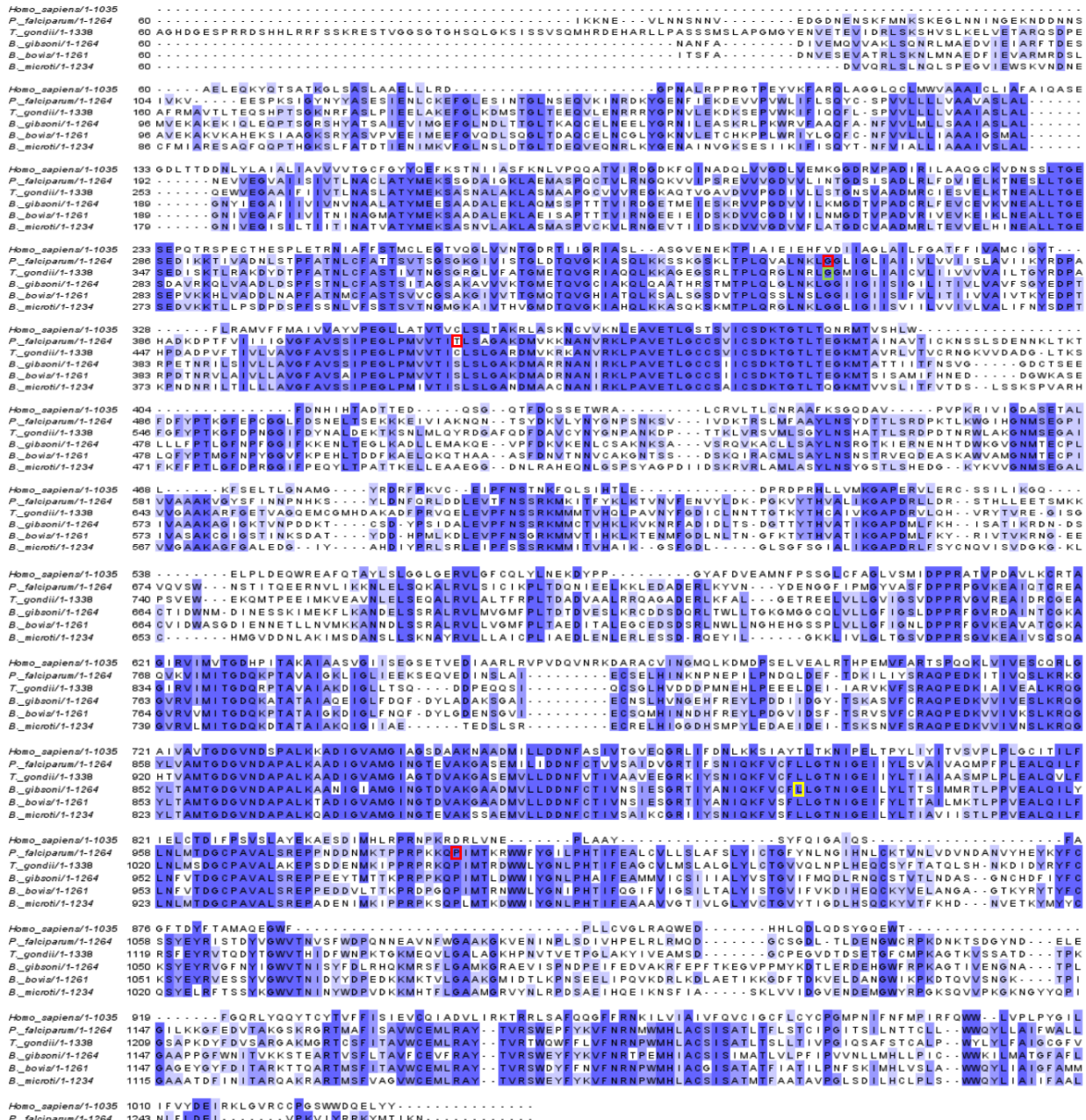

Figure supplement 2. Multiple sequence alignment of ATP4 in different species. A yellow square denotes the *Bg*ATP4 mutation site discovered in this investigation; red squares represent sites linked to *P. falciparum* CIP resistance, and a green square represents sites associated with *T. gondii*.

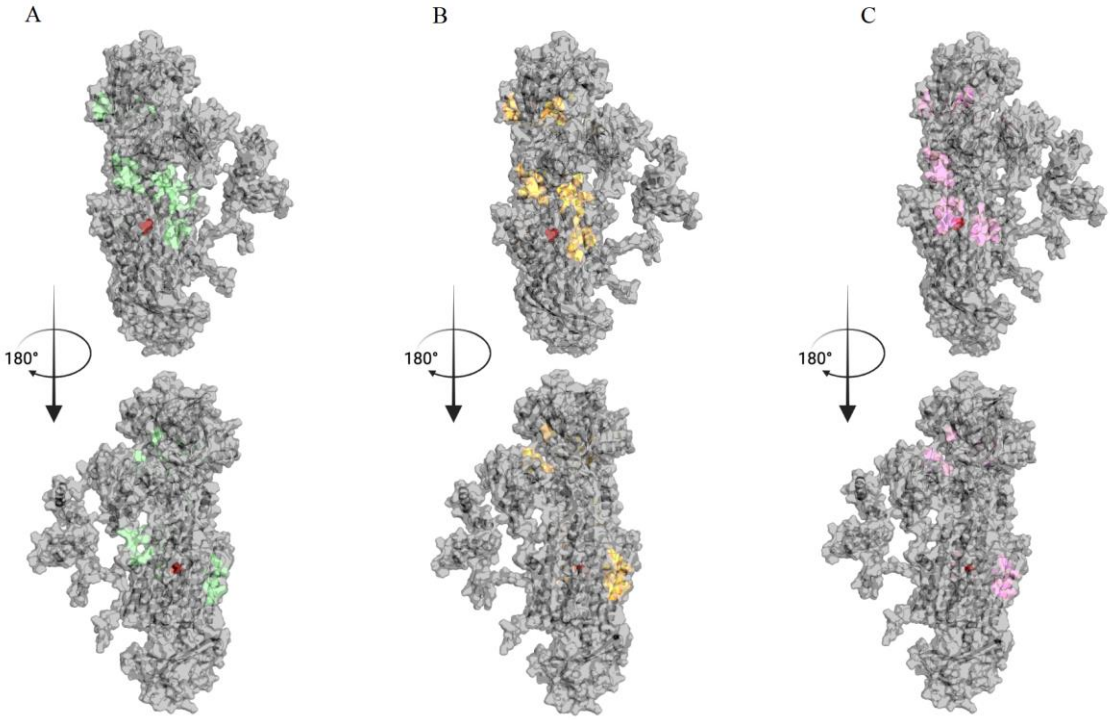

Figure supplement 3. Binding sites for CIP found by Gnina search across the entire surface of the protein. (**A-C**) The binding space of WT, L921V, and L921I mutants in *Bg*ATP4 are labeled in green, yellow and pink, respectively.

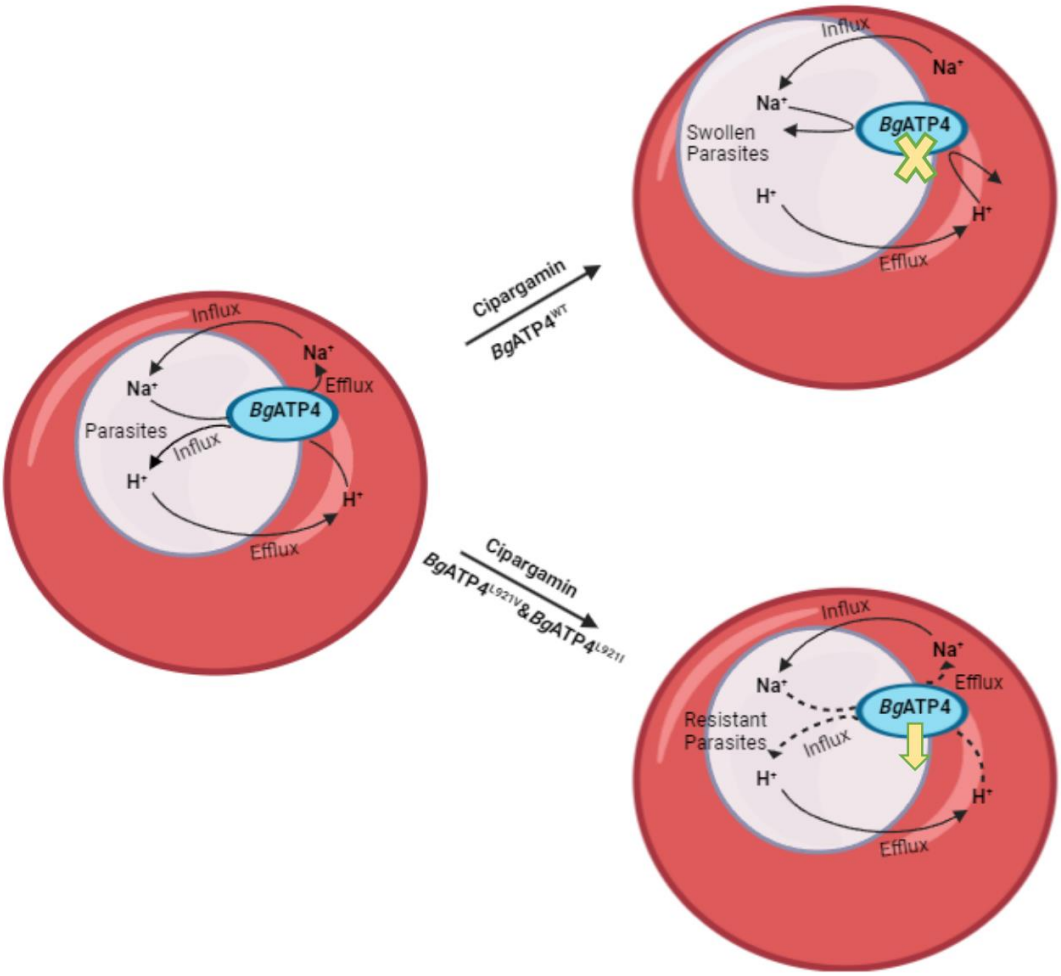

Figure supplement 4. Proposed mechanism of inhibition of CIP on wild-type and mutant parasite-infected erythrocytes. CIP disrupts the *Bg*ATP4 function of wild-type parasites, which causes a net influx of Na^+ and efflux of H^+ from the parasite. The osmotic load imposed on the influx of Na^+ further brings about parasite swelling and internal alkalinization, which are the main factors in *Babesia* death. Mutations in ATP4 minimize the susceptibility to ATP4 inhibitors by recovering H^+ and Na^+ balance.

Supplemental Tables

Table supplement 1. Primer sets of *B. gibsoni* ATP4

Gene	Primer (5'-3')
*Bg*ATP4 1F	ACGTAGTTGTCGAACATCTTACACCAATGC
*Bg*ATP4 1R	CAGAGGTAGCATAGTGAGATCGCCCCGA
*Bg*ATP4 2F	GAGATTGCAAGGTTTACGGATGAGTCTATGG
*Bg*ATP4 2R	ATGACAACGTCACCGGGTACAACACGCTTG
*Bg*ATP4 3F	GAAAAGCTTGCTCAAATGTCTTCACCGACAAC
*Bg*ATP4 3R	GTTTCTGGACGAGTTGGATCCTCATAACC
*Bg*ATP4 4F	AAATTGGGGGGGATAATTGGCATTATCTCC
*Bg*ATP4 4R	ACCTTATCAAAGGGTACCTCTTGCTTTG
*Bg*ATP4 5F	TCAATCCATTCGGTGGAATTTTCAAAAAGG
*Bg*ATP4 5R	GTGTTTGAATAACATATCTGGTGCCCCCTT
*Bg*ATP4 6F	GGTAAAGAACAGATTTGCTGACATAGATCT
*Bg*ATP4 6R	ACCCTATTTCTTGTGCGATGGCCGTAGCTG
*Bg*ATP4 7F	AGGGACGCTATAAATACTTGTGGAAAGGC
*Bg*ATP4 7R	GTACGCCCAGACTCGATTGAGTTAACTATTG
*Bg*ATP4 8F	GGGTATTAATGGCACAGATGTTGCAAAAGG
*Bg*ATP4 8R	GACAGTTCCCACTAGCATCATTAAGTGTAA
*Bg*ATP4 9F	ATCATCATTGCGCTATATGTTTCTACCGG
*Bg*ATP4 9R	CTAATGGGGTAGCATTTCCATTCTCAACAA
*Bg*ATP4 10F	AGGGAGTTCCTCCCATGTATAAAGATACCT
*Bg*ATP4 10R	TTAGGCTTCTGCCCTTTTCATTTTTCGCTT

578 **Table supplement 2.** Interactions of CIP from docking simulations

Receptor	Name	Distance	Category	Types
*Bg*ATP4^{WT}	GLY407	2.67648	Hydrogen Bond; Halogen	Carbon Hydrogen Bond; Halogen (Fluorine)
	CYS959	3.2396	Halogen	Halogen (Cl, Br, I)
	VAL962	2.66882	Hydrophobic	Pi-Sigma
	CYS959	4.38742	Hydrophobic	Alkyl
	VAL962	4.29249	Hydrophobic	Alkyl
	ALA963	3.8231	Hydrophobic	Alkyl
	ALA1202	3.67015	Hydrophobic	Alkyl
	MET211	5.06565	Hydrophobic	Alkyl
	VAL962	4.25668	Hydrophobic	Alkyl
	ILE414	4.70605	Hydrophobic	Alkyl
	CYS959	4.83891	Hydrophobic	Pi-Alkyl
	VAL962	4.98402	Hydrophobic	Pi-Alkyl
	VAL411	5.43239	Hydrophobic	Pi-Alkyl
	VAL962	5.05537	Hydrophobic	Pi-Alkyl
	PHE954	4.07586	Hydrophobic	Pi-Alkyl
*Bg*ATP4^{L921V}	GLY407	2.69013	Hydrogen Bond; Halogen	Carbon Hydrogen Bond; Halogen (Fluorine)
	CYS959	3.22066	Halogen	Halogen (Cl, Br, I)
	VAL962	2.66391	Hydrophobic	Pi-Sigma
	CYS959	4.35422	Hydrophobic	Alkyl
	VAL962	4.31879	Hydrophobic	Alkyl
	ALA963	3.8209	Hydrophobic	Alkyl
	ALA1202	3.63038	Hydrophobic	Alkyl
	MET211	5.0878	Hydrophobic	Alkyl
	VAL962	4.24186	Hydrophobic	Alkyl
	ILE414	4.71819	Hydrophobic	Alkyl
	CYS959	4.82036	Hydrophobic	Pi-Alkyl
	VAL962	4.99879	Hydrophobic	Pi-Alkyl
	VAL411	5.4334	Hydrophobic	Pi-Alkyl
	VAL962	5.04532	Hydrophobic	Pi-Alkyl
	PHE954	4.07482	Hydrophobic	Pi-Alkyl
*Bg*ATP4^{L921I}	GLY958	2.92346	Hydrogen Bond; Halogen	Carbon Hydrogen Bond; Halogen (Fluorine)
	GLY958	3.3301	Halogen	Halogen (Fluorine)
	MET410	5.88505	Other	Pi-Sulfur
	VAL955	4.31406	Hydrophobic	Alkyl

MET410	3.69023	Hydrophobic	Alkyl
VAL411	4.83101	Hydrophobic	Alkyl
VAL955	4.79513	Hydrophobic	Alkyl
VAL955	4.84729	Hydrophobic	Alkyl
CYS959	4.1269	Hydrophobic	Alkyl
ILE1205	4.82529	Hydrophobic	Alkyl
CYS959	5.21399	Hydrophobic	Alkyl
VAL955	4.90527	Hydrophobic	Pi-Alkyl
PHE954	5.03012	Hydrophobic	Pi-Alkyl